

Commun. Theor. Phys. **75** (2023) 125405 (9pp) https://doi.org/10.1088/1572-9494/ad0bf3

Heat engines of the Kerr-AdS black hole

Yi Zhong[1] **and Yun-Zhi Du**[2,3,*]

[1] School of Physics and Electronics, Hunan University, Changsha 410082, China
[2] Department of Physics, Shanxi Datong University, Datong 037009, China
[3] Institute of Theoretical Physics, Shanxi Datong University, Datong 037009, China

E-mail: zhongy@hnu.edu.cn and duyzh22@sxdtdx.edu.cn

Received 19 September 2023, revised 24 October 2023
Accepted for publication 13 November 2023
Published 20 December 2023

Abstract

In this paper, we investigate three types of heat engines for the rotating Kerr-Anti de Sitter (Kerr-AdS) black hole. We first briefly review the thermodynamics and phase structure of the Kerr-AdS black hole and obtain the phase structure in the T–S chart. The thermal stability of Kerr-AdS black holes, along with their dependence on various parameters, is thoroughly examined. Then, by utilizing the phase diagram, we consider three types of heat engines: the maximal Carnot engine, Stirling engine, and Rankine engine. We calculate both the work and efficiency for these engines. The results indicate that angular momentum has a significant influence on these heat engines.

Keywords: black hole, heat engine, Kerr-AdS

(Some figures may appear in colour only in the online journal)

1. Introduction

Black hole thermodynamics is an interesting and fascinating topic in gravitational physics. Particularly, in the extended phase space, the cosmological constant can be treated as a new variable, representing the pressure of the gravitational system [1–9]. Meanwhile, the black hole mass is interpreted as the enthalpy of the system. After this proposal, the black hole system can be cast to be an ordinary thermodynamic system, which has temperature, pressure, and volume, as well as the microscopic structure [10]. And this has raised a great interest in the study of black hole phase transitions and critical phenomena.

Among the study of Anti-de Sitter (AdS) black hole thermodynamics, the black hole heat engine has become an important implement since the black hole heat engine can be helpful for understanding classical and quantum aspects of gravity. This work was initiated by Johnson in [11]. The author first constructed an engine with two isobars and two isochores. In the high-temperature limit, they obtained the heat, work, and efficiency for the engine. The author also provided a precise framework for expanding the traditional, thermodynamic dictionary of holography. The engine cycles were also expected to be performed with the renormalization group flow. Subsequently, by making use of the first law of black hole thermodynamics, an exact efficiency formula was obtained in [12]. The study of this black hole engine was further extended to other black hole systems [13–37].

For an engine, efficiency is a key quantity. So, how to increase efficiency is an important question. Although different kinds of engines have different efficiencies, the study of the efficiency of the Carnot engine may provide us with valuable insights. As is well known, all reversible heat engines working between the same two heat sources, including the Carnot engine, have the same efficiency, which is

$$\eta_{\mathrm{C}} = 1 - \frac{T_2}{T_1}, \tag{1.1}$$

with T_1 and T_2 being the high and low temperatures of the heat sources, respectively. So raising the efficiency can be achieved by increasing T_1 or decreasing T_2. However, modifying the temperature can lead to some new questions of the system, which should be included. For example, if one continues to decrease the low temperature T_2 for the charged AdS black hole, then the critical temperature is approached. And below it, the black hole system will exhibit a small-large black hole phase transition. When the black hole system crosses the phase transition point, the latent heat will be released or absorbed [10]. So such a black hole phase structure must be included.

After considering the black hole phase structure, a new black hole engine modeled with the Rankine cycle for the charged AdS black hole was proposed [36]. For each cycle, the system will experience two small-large black hole phase

* Author to whom any correspondence should be addressed.

transitions. By fixing the low temperature T_2, it was found that there will be more useful work and low efficiency at low T_1. However, at high T_1, the efficiency is high, but the useful work is less. So, a large amount of work and high efficiency can not be realized at the same time. In order to overcome this difficulty, a back pressure mechanism was introduced. The detailed properties of this back pressure Rankine (BPR) cycle were thoroughly examined in [36]. Furthermore, this study was also generalized to the higher-dimensional charged AdS black hole [37]. The work and efficiency of the black hole engine increases rapidly as the number of spacetime dimensions grows. Therefore, the higher-dimensional charged AdS black hole can act as a more efficient power plant to produce the mechanical work.

Compared to the charged AdS black hole, a four-dimensional rotating Kerr-AdS black hole also exhibits a small-large black hole phase transition similar to the van de Waals (vdW) fluid [38, 39]. One intriguing property of the rotating AdS black hole is that its adiabatic process is different from the isometric process, which leads to the difference between the Carnot cycle and the Stirling cycle [11]. This is a significant difference from the charged one. So it is interesting to consider the heat engine of the rotating AdS black hole, and to determine the influence of the angular momentum on the engine physics. The efficiency for the Carnot cycle of the Kerr-Sen-AdS black hole, which recovers the Kerr-AdS when the charge vanishes, was investigated in [40]. We will further investigate the Stirling engine and the Rankine engine.

This work is organized as follows. In section 2, we briefly review the thermodynamics for the Kerr-AdS black hole. The phase structure in the T–S chart is obtained. Employing the first law of the black hole, we study the heat absorbed or released during four kinds of thermodynamic processes in section 3. Then based on the phase structure, we investigate three kinds of black hole heat engines, i.e., the maximal Carnot engine, the Stirling engine, and the Rankine engine in section 4.1. The influence of the angular momentum on the mechanical work and efficiency of the black hole engines are analyzed. The last section is devoted to conclusions.

2. Thermodynamics and phase transition of Kerr-AdS black hole

In this section, we will provide a concise overview of the thermodynamics and phase structure of the Kerr-AdS black hole. For more in-depth exploration of recent developments in this field, we refer readers to the [41, 42]

The line element of the rotating Kerr-AdS black hole is

$$\begin{aligned} ds^2 =& -\frac{\Delta}{\rho^2}\left(dt - \frac{a\sin^2\theta}{\Xi}d\varphi\right)^2 \\ &+ \frac{\rho^2}{\Delta}dr^2 + \frac{\rho^2}{1 - a^2/l^2\cos^2\theta}d\theta^2 \\ &+ \frac{(1 - a^2/l^2\cos^2\theta)\sin^2\theta}{\rho^2}\left(adt - \frac{r^2 + a^2}{\Xi}d\varphi\right)^2, \end{aligned} \tag{2.1}$$

where the metric functions read

$$\rho^2 = r^2 + a^2\cos^2\theta, \quad \Xi = 1 - \frac{a^2}{l^2}, \tag{2.2}$$

$$\Delta = (r^2 + a^2)(1 + r^2/l^2) - 2mr, \tag{2.3}$$

and l is the AdS curvature radius. The black hole mass M and angular momentum J are related to the parameters m and a as

$$M = \frac{m}{\Xi^2}, \quad J = \frac{am}{\Xi^2}. \tag{2.4}$$

The temperature, entropy and angular velocity are given by

$$T = \frac{r_h}{4\pi(r_h^2 + a^2)}\left(1 + \frac{a^2}{l^2} + 3\frac{r_h^2}{l^2} - \frac{a^2}{r_h^2}\right), \tag{2.5}$$

$$S = \frac{\pi(r_h^2 + a^2)}{\Xi}, \quad \Omega = \frac{a\Xi}{r_h^2 + a^2} + \frac{a}{l^2}, \tag{2.6}$$

with r_h the outer horizon radius of the black hole. The black hole mass M and angular momentum J are related to the parameters m and a as

$$M = \frac{m}{\Xi^2}, \quad J = \frac{am}{\Xi^2}. \tag{2.7}$$

The Gibbs free energy of the black hole is

$$\begin{aligned} G =& M - TS \\ =& \frac{a^4(r_h^2 - l^2) + a^2(3l^4 + 2l^2r_h^2 + 3r_h^4) + l^2r_h^2(l^2 - r_h^2)}{4r_h(a^2 - l^2)^2}. \end{aligned} \tag{2.8}$$

In our approach, we treat the cosmological constant as the thermodynamic pressure [4]

$$P = -\frac{\Lambda}{8\pi} = \frac{3}{8\pi l^2}. \tag{2.9}$$

Solving the entropy and angular momentum in (2.6) and (2.4), we have

$$r_h = \sqrt{\frac{S^3(8PS + 3)}{\pi(12\pi^2J^2 + S^2(8PS + 3))}}, \tag{2.10}$$

$$a = 6J\sqrt{\frac{\pi S}{(8PS + 3)(12\pi^2J^2 + S^2(8PS + 3))}}. \tag{2.11}$$

The black hole mass in our approach should be treated as the enthalpy of the system, and we can express it as

$$H \equiv M = \frac{\sqrt{(8PS + 3)(12\pi^2J^2 + S^2(8PS + 3))}}{6\sqrt{\pi S}}. \tag{2.12}$$

The energy of the black hole system should be $U = H - PV$, which gives

$$U = \frac{4\pi^2J^2(4PS + 3) + S^2(8PS + 3)}{2\sqrt{\pi S}\sqrt{(8PS + 3)(12\pi^2J^2 + S^2(8PS + 3))}}. \tag{2.13}$$

Moreover, the temperature, Gibbs free energy, and thermodynamic volume can also be re-expressed in terms of S, J, and P:

$$T = \frac{S^2(64P^2S^2 + 32PS + 3) - 12\pi^2J^2}{4\sqrt{\pi}S^{3/2}\sqrt{8PS + 3}\sqrt{12\pi^2J^2 + S^2(8PS + 3)}}, \tag{2.14}$$

$$G = \frac{12\pi^2 J^2(16PS+9) - 64P^2S^4 + 9S^2}{12\sqrt{\pi}\sqrt{S}\sqrt{8PS+3}\sqrt{12\pi^2J^2 + S^2(8PS+3)}}, \tag{2.15}$$

$$V = \frac{4\sqrt{S}(6\pi^2J^2 + S^2(8PS+3))}{3\sqrt{\pi}\sqrt{8PS+3}\sqrt{12\pi^2J^2 + S^2(8PS+3)}}. \tag{2.16}$$

In general, the heat capacity indicates a local thermodynamic stability: positive (negative) heat capacity corresponds to the stable (unstable) system. It should also be noted that the information of the black hole phase transition is encoded in the heat capacity. For the rotating Kerr-AdS black hole, the heat capacity at fixed J and P is given by

$$\begin{aligned} C_{J,P} &= T\left(\frac{\partial S}{\partial T}\right)_{J,P} \\ &= \frac{2S(8PS+3)(12\pi^2J^2 + S^2(8PS+3))(S^2(8PS+1)(8PS+3) - 12\pi^2J^2)}{144\pi^4J^4(32PS+9) + 24\pi^2J^2S^2(8PS+3)^2(16PS+3) + S^4(8PS-1)(8PS+3)^3}. \end{aligned} \tag{2.17}$$

We present plots depicting the heat capacity as a function of both J and P to illustrate the thermal stability of this system, as shown in figure 1. For a fixed value of J or P, there exists three phases for different values of P or J: the large/small black hole phases are locally stable, while the intermediate phase is unstable. As P or J increases, the gap between the locally stable large/small black hole phases decrease as the first-order transition point shifts to the right, with the appearance of a second-order transition point. These results are the same as those reported for charged rotating Kerr-Sen-AdS black holes in [41].

On the other hand, it has been reported that there exists a small-large black hole phase transition in the four-dimensional Kerr-AdS black hole background [38, 39]. And the exact critical point was given in [43]. Such a phase transition can be easily studied in the T–S chart rather than the P–V chart. The oscillatory behavior of the isobaric lines is shown in figure 2. Clearly, the oscillatory behavior indicates a phase transition. Such phase transition is of the vdW type. And the critical point is given by [43]

$$\begin{aligned} &P_c = \frac{0.002857}{J}, \quad T_c = 6.047357\sqrt{J}, \\ &V_c = 115.796503\sqrt[3]{J}. \end{aligned} \tag{2.18}$$

By constructing the equal area law, we obtain the parametrization form of the coexistence curve [43]

$$\begin{aligned} \tilde{P} = {} & 0.718781\tilde{T}^2 + 0.188586\tilde{T}^3 + 0.061488\tilde{T}^4 \\ & + 0.022704\tilde{T}^5 + 0.002340\tilde{T}^6 \\ & + 0.010547\tilde{T}^7 - 0.008649\tilde{T}^8 + 0.005919 \\ & \tilde{T}^9 - 0.001717\tilde{T}^{10}, \quad \tilde{T} \in (0, 1), \end{aligned} \tag{2.19}$$

where $\tilde{P} = \frac{P}{P_c}$ and $\tilde{T} = \frac{T}{T_c}$. Using this parametrization form, we can obtain the phase diagram in the T–S chart. For the fixed $J = 0.1$, the phase structure is displayed in figure 3. There are four phases in this picture. Regions I and III are for the small and large black hole phases, respectively. Region IV is above the critical point, and we denote it as the supercritical phase. While region I, below the curve, represents the coexistence phase of the small and large black holes. Specifically, the left blue curve corresponds to the saturated small black hole, and the right red curve corresponds to the saturated large black hole. For a fixed temperature lower than the critical temperature, the system will encounter the small black hole phase, coexistence phase, and large black hole phase with the increase of the entropy. The phase transition occurs when it crosses the blue and red curves. Such phase transition is a first-order phase transition.

Next, we consider thermodynamic processes that will be employed in the heat engine for this study.

3. Thermodynamic processes

For the four-dimensional Kerr-AdS black hole, the first law reads

$$\mathrm{d}U = T\mathrm{d}S + \Omega\mathrm{d}J - P\mathrm{d}V, \tag{3.1}$$

$$\mathrm{d}H = T\mathrm{d}S + \Omega\mathrm{d}J + V\mathrm{d}P. \tag{3.2}$$

During an infinitesimal thermodynamic process, the system will exchange heat Q and work W with its surroundings, which are measured with

$$dQ = T\mathrm{d}S, \quad dW = \Omega\mathrm{d}J - P\mathrm{d}V. \tag{3.3}$$

Note that heat and work are not state functions. In a finite thermodynamic process, they can be calculated with an integral. The heat absorbed or released in a process can also be measured with the heat capacity, which is defined as

$$C_{J,P} = \left(\frac{\partial U}{\partial T}\right)_{J,P} = T\left(\frac{\partial S}{\partial T}\right)_{J,P}, \tag{3.4}$$

where the subscripts J and P represent that J and P are constant when taking partial derivatives. In the second step, we have used the first law (3.1). Then the heat can be measured with

$$\mathrm{d}Q = C_{J,P}\mathrm{d}T. \tag{3.5}$$

Since the energy U is a state function, we have a closed thermodynamic process,

$$\Delta U = 0, \tag{3.6}$$

which leads to the result

$$\Delta Q + \Delta W = 0. \tag{3.7}$$

Based on this formula, calculating the heat in a closed cycle also allows us to determine the associated work.

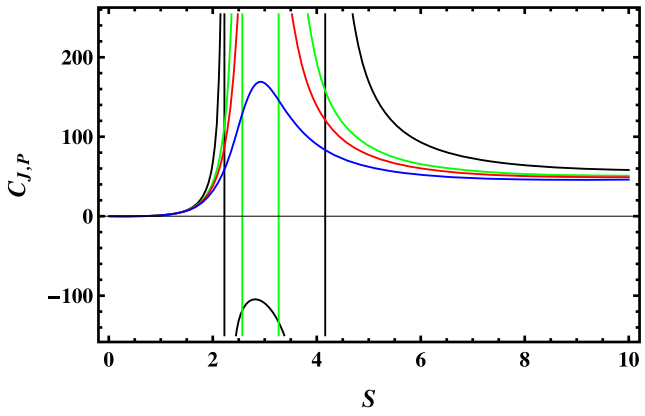

(a) J=0.1

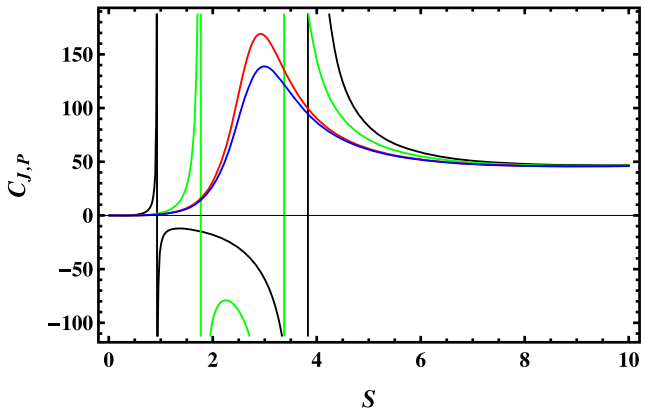

(b) P=0.031

Figure 1. Plots of the heat capacity with different angular momentum J and pressure P. (a) $J = 0.1$, and $P = 0.025$, 0.028, 0.029, and 0.031 from bottom to top. (b) $P = 0.031$, and $J = 0.05$, 0.08, 0.1, and 0.102 from bottom to top.

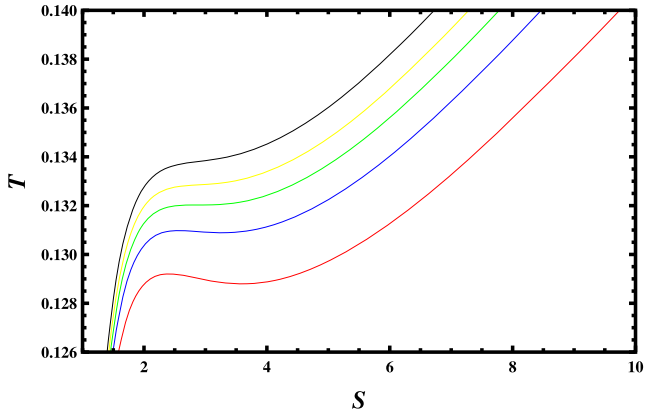

(a) J=0.1

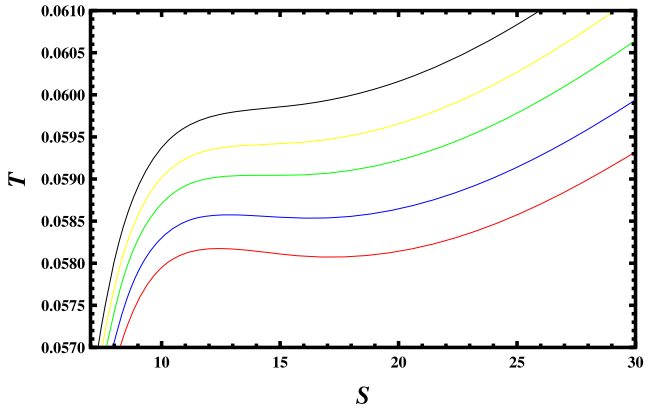

(b) J=0.5

Figure 2. Isobaric curves in the T–S chart with fixed angular momentum J. (a) $J = 0.1$, and $P = 0.027$, 0.028, 0.028 57, 0.029, and 0.0295 from bottom to top. (b) $J = 0.5$, and $P = 0.0055$, 0.0056, 0.005 174, 0.0058, and 0.0059 from bottom to top.

Consequently, our focus here is on the calculation of heat. As illustrated earlier, heat in an infinitesimal thermodynamic process is typically quantified using either (3.3) or (3.5). In this context, we prefer employing the formula (3.3). The subsequent subsections will primarily delve into heat analysis within the T–S chart for four distinct processes.

3.1. Adiabatic process

In the T–S chart, the adiabatic process corresponds to a vertical line. Thus, the heat for it is

$$\Delta Q = 0. \tag{3.8}$$

3.2. Isothermal process

It is also obvious that the isothermal process is a horizontal line in the T–S chart, so the heat is

$$\Delta Q = \int_{S_1}^{S_2} T\mathrm{d}S = T\Delta S, \tag{3.9}$$

which is just the rectangular area under the horizontal line.

3.3. Isobaric process

For the isobaric process, the heat is

$$\Delta Q = \int_{S_1}^{S_2} T\mathrm{d}S, \tag{3.10}$$

which is measured with the area under the curve. On the other hand, the first law will be of the form

$$\mathrm{d}H = T\mathrm{d}S + \Omega\mathrm{d}J. \tag{3.11}$$

If the angular momentum J is fixed during this process, we will get

$$\mathrm{d}H = T\mathrm{d}S = \mathrm{d}Q, \tag{3.12}$$

which means the heat coincides with the enthalpy, so one easily has

$$\Delta Q = \Delta H. \tag{3.13}$$

3.4. Isometric process

In an isometric process, the change of the volume $\Delta V = 0$. The heat absorbed or released in it is also measured with the area under that curve. Moreover, if we fix the angular

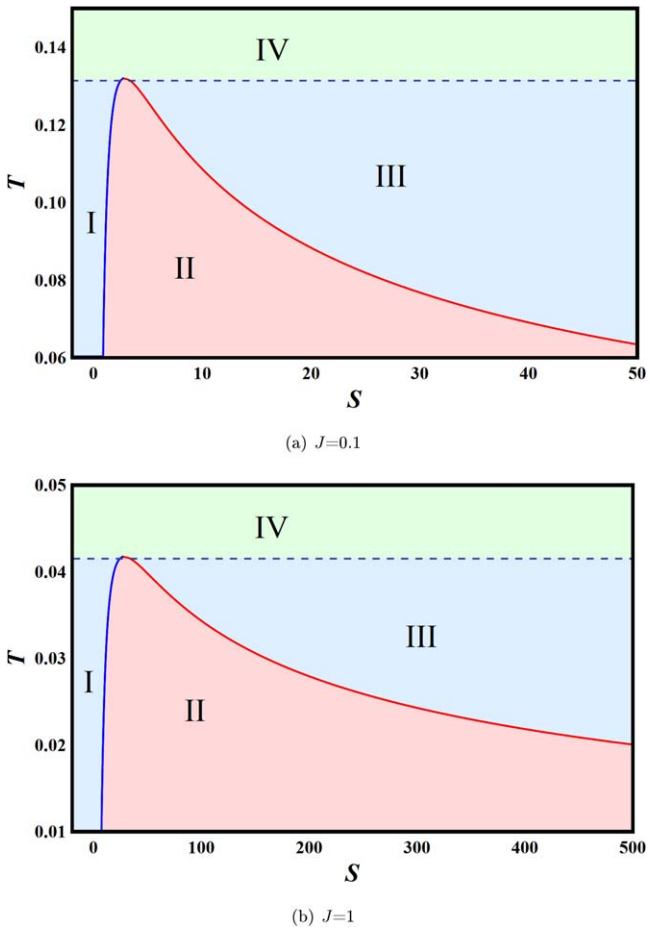

Figure 3. Phase diagram for the Kerr-AdS black hole. (a) $J = 0.1$. (b) $J = 1$.

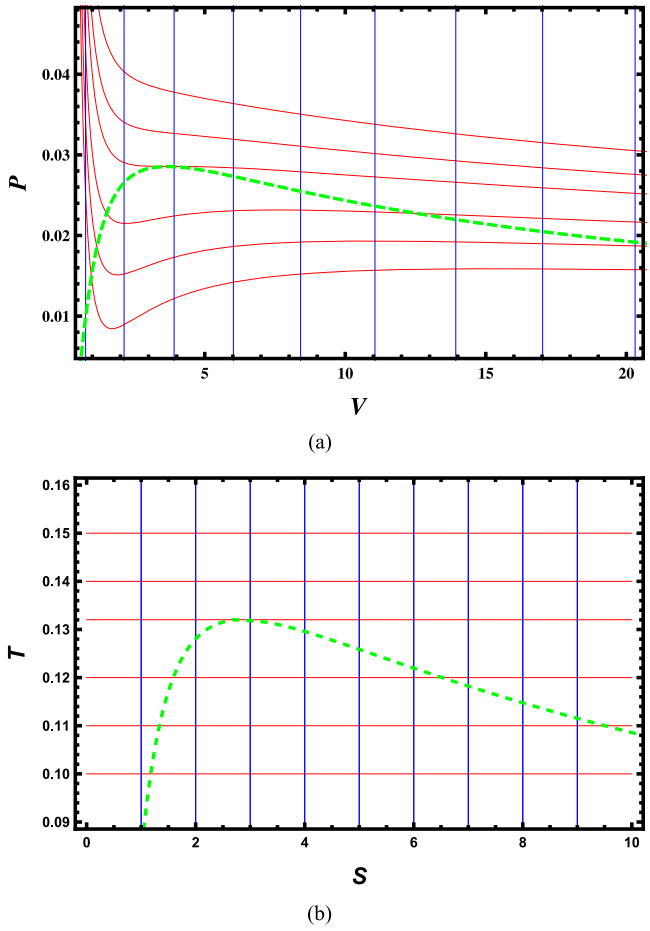

Figure 4. Isothermal curves (red lines) and adiabatic curves (blue lines) for the Kerr-AdS black hole with $J = 0.1$. (a) P–V chart. The temperature $T = 0.1$, 0.11, 0.12, T_c, 0.14, 0.15 from bottom to top, and the entropy $S = 1$, 2, 3, 4, 5, 6, 7, 8, 9 from left to right. (b) T-S chart. The dashed green curve denotes the saturated small and large black holes, below which is the coexistence phase of small and large black holes.

momentum J, then we easily have

$$\mathrm{d}U = T\mathrm{d}S. \tag{3.14}$$

Thus

$$\Delta Q = \Delta U. \tag{3.15}$$

4. Heat engines

A heat engine is a cyclic device operating in a closed thermodynamic process, exchanging only heat and work with its surroundings. Typically, the choice of the thermodynamic cycle for a heat engine depends on the properties of the working substance. In this case, we are considering the black hole as the working substance, whose phase structure has been discussed previously. Our focus is primarily on three types of heat engines: the Carnot engine, the Stirling engine, and the Rankine engine. Previous research on these engines has mainly focused on high-temperature conditions, beyond the phase transition. In this study, we aim to incorporate the phase transition into our analysis. In the case of a simple heat engine, it exhibits two key characteristics: a heat source at a high temperature and a heat sink at a lower temperature. We denote Q_1 and Q_2 as the heat absorbed by the engine from the high-temperature source and the heat sink, respectively. Additionally, we use W to represent the work done by the surroundings on the engine during each cycle. Then, equation (3.7) can be expressed as

$$Q_1 + Q_2 + W = 0. \tag{4.1}$$

Note that Q_1 is positive, while Q_2 and W are negative in our notation. Then the efficiency for a heat engine will be

$$\eta = -\frac{W}{Q_1} = 1 + \frac{Q_2}{Q_1}. \tag{4.2}$$

4.1. Carnot engine

The Carnot engine, conceived by Carnot in 1824, is the simplest design. Its thermodynamic cycle contains four reversible steps, two isothermal steps and two adiabatic steps. We show the isothermal curves and adiabatic curves in the P–V and T–S charts in figure 4. Each small closed cycle can serve as a Carnot engine. From the T–S chart, we can easily

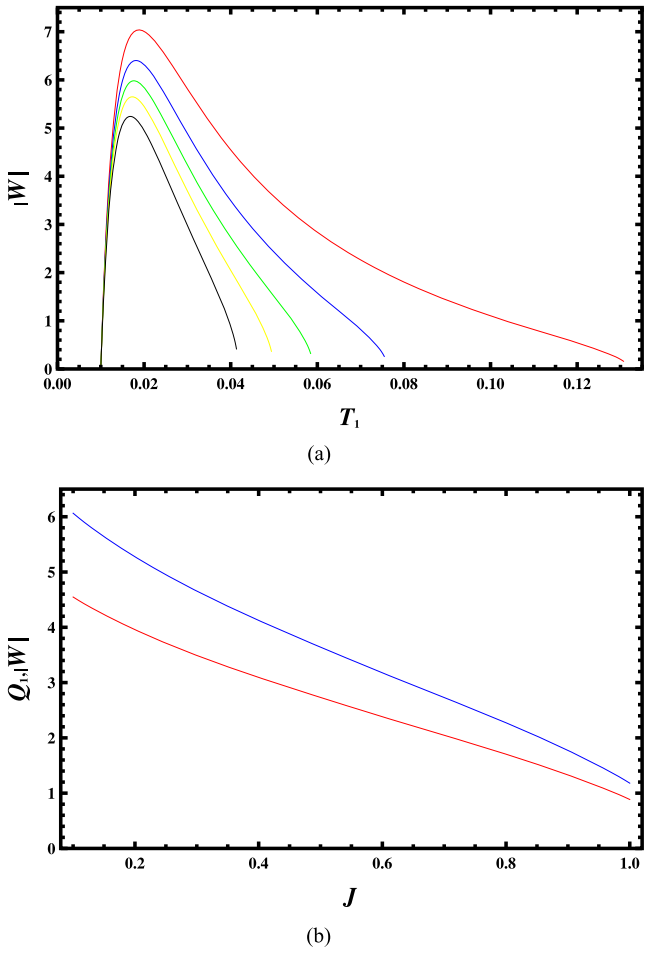

Figure 5. (a) Work as a function of the high temperature T_1 for the maximal Carnot cycle with the low temperature set to $T_2 = 0.01$. From top to bottom, the angular momentum $J = 0.1$, 0.3, 0.5, 0.7, and 1. (b) The heat (top blue line) and work (bottom red line) as a function of the angular momentum J for the maximal Carnot cycle with a low temperature $T_2 = 0.01$ and a high temperature $T_1 = 0.04$.

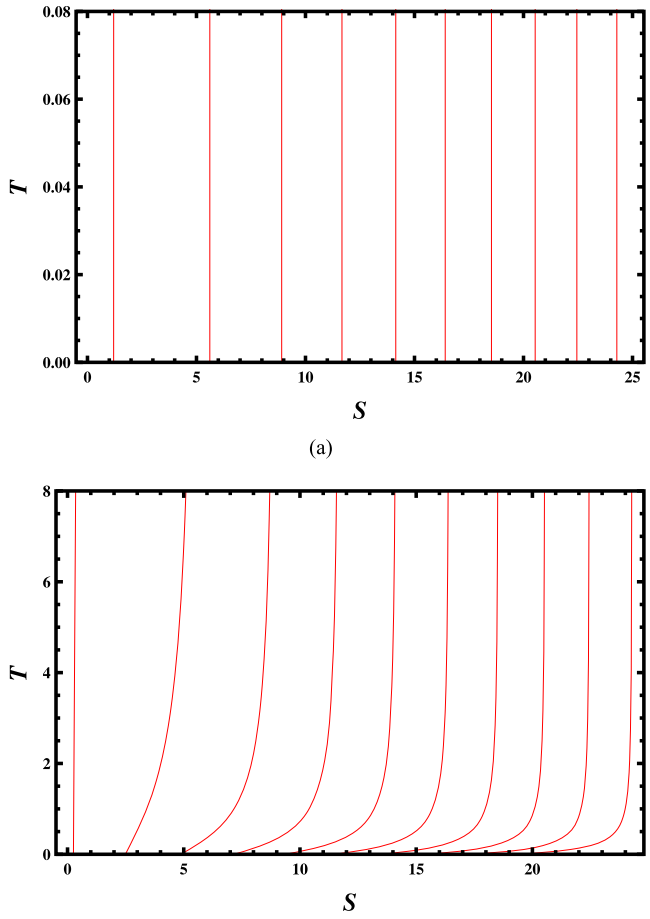

Figure 6. Isometric curves in the T–S chart. The volume $V = 1$, 10, 20, 30, 40, 50, 60, 70, 80, and 90 from left to right. (a) $J = 0.1$. (b) $J = 10$.

read out that the efficiency for the heat engine is

$$\eta = 1 - \frac{T_2}{T_1}. \tag{4.3}$$

For a specific engine, we aim to study the maximum Carnot cycle, even though the efficiency is given in (4.3). During this cycle, the black hole is always in a coexistence phase. A sketch of such a thermodynamic cycle can be found in [36]. First, we fix the low temperature $T_2 = 0.01$, and allow the high temperature T_1 to vary from T_2 to its critical point. The work W is shown in figure 5(a) for the angular momentum $J = 0.1$, 0.3, 0.5, 0.7, and 1. For each curve, the work firstly starts at zero, then approaches its maximum, and decreases to zero when the critical temperature is reached. We can also find that the peak of the work decreases with the angular momentum, and it slightly shifts to a lower temperature.

Moreover, we can fix the low and high temperatures simultaneously, after which the heat and work can be calculated. Here we set $T_1 = 0.04$ and $T_2 = 0.01$, the result is depicted in figure 5(b). It is obvious that both the heat and work are monotone functions of the angular momentum J. So when the low and high temperatures are fixed, lowering the angular momentum will produce a large amount of work.

4.2. Stirling engine

Compared to the Carnot engine, the two adiabatic steps are replaced with two isometric steps for the Stirling engine. For the charged AdS black hole, the adiabatic process coincides with its isometric process, so the Carnot cycle and the Stirling cycle coincide with each other [11]. However, for the Kerr-AdS black hole, the two cycles are different. Thus, it is interesting to study the Stirling engine for the Kerr-AdS black hole. Here we plot the isometric curves in the T–S chart in figure 6. It is surprising that for the small angular momentum $J = 0.1$, the isometric curves are almost vertical lines, similar to the adiabatic curves. However, for a large angular momentum $J = 10$, we observe the difference at low temperature.

According to the definition of the efficiency, the Stirling cycle shares the same efficiency (4.2) as the Carnot cycle. We also consider the maximum cycle that the working substance is in a coexistence phase for during one cycle. And only two

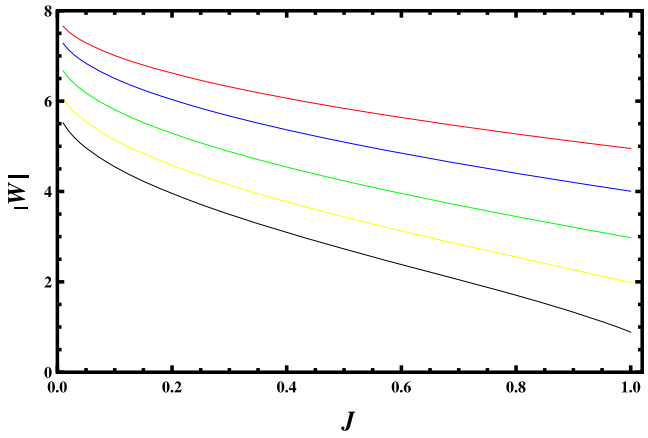

Figure 7. Work for the Stirling cycle as a function of the angular momentum. The low temperature is set to $T_2 = 0.01$ and the high temperature $T_1 = 0.02, 0.025, 0.030, 0.035, 0.04$ from top to bottom.

vertices are located on the saturated small and large black holes. The work for each cycle can be calculated with

$$|W| = (S(T_1, V_1) - S(T_1, V_2))T_1 - (S(T_2, V_2) - S(T_2, V_1))T_2. \tag{4.4}$$

We present the work for the Stirling cycle with fixed low and high temperatures in figure 7. The low temperature is set to $T_2 = 0.01$, and the high temperature $T_1 = 0.02, 0.025, 0.030, 0.035, 0.04$ from top to bottom. From figure 7, we see that the amount of the work decreases with the angular momentum J. Moreover, for the same J, the work decreases with the high temperature.

4.3. Rankine engine

A practical and widely used heat engine is the steam power plant, which can be modeled with a Rankine cycle. For the black hole, the cycle was first studied in [36] by utilizing the phase structure for a charged AdS black hole. The sketch picture for that cycle can be found in [36]. The study reveals that the introduction of the back pressure mechanism for the Rankine engine yields the highest efficiency, so we will study the cycle with a back pressure mechanism for the Kerr-AdS black hole.

The heat absorbed from the heat source, work and the efficiency for the black hole are [36]

$$Q_1 = \text{area(JBCDEHJ)}, \tag{4.5}$$

$$|W| = \text{area(ABCDEFA)} \tag{4.6}$$

$$\eta = 1 - \frac{H_{J,P_A}(S_F) - H_{J,P_A}(S_A)}{H_{J,P_B}(S_F) - H_{J,P_B}(S_A)}, \tag{4.7}$$

where area(JBCDEHJ) and area(ABCDEFA) are areas in the T–S chart in [36]. We fix the low temperature T_2 and allow the high temperature to vary from the low temperature to its critical point. Then we obtain the work and efficiency for the black hole during each cycle. The result is presented in figure 8. For fixed angular momentum J, we can see that the amount of the work and the efficiency of the engine increases

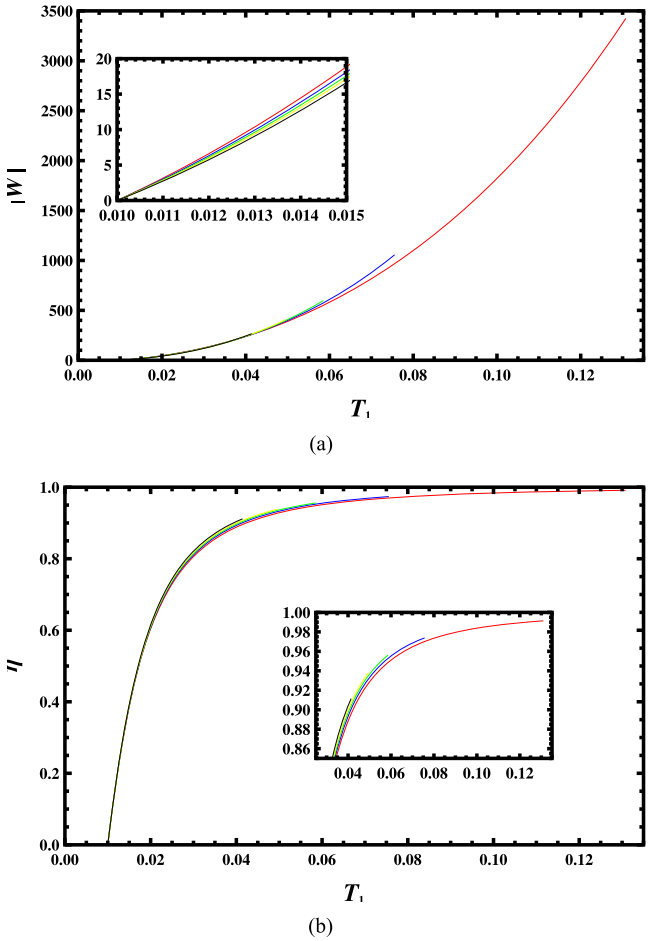

Figure 8. Work and efficiency for the Rankine engine with the low temperature $T_2 = 0.01$. (a) Work versus high temperature T_1 with the angular momentum $J = 0.1, 0.3, 0.5, 0.7$, and 1 from top to bottom. (b) Efficiency versus high temperature T_1 with $J = 0.1, 0.3, 0.5, 0.7$, and 1 from bottom to top.

with T_1. And for low T_1, the work slightly decreases with the angular momentum J, while the efficiency increases with it. Moreover, since small J produces high critical temperature, we can achieve a large amount of work and a high efficiency near the critical temperature, for example $|W| = 3407$ and $\eta = 0.9912$ for $J = 0.1$.

Interestingly, we can also fix the low and high temperatures simultaneously. The numerical result is shown in figure 9. The low temperature is set to $T_2 = 0.01$, and the high temperature $T_1 = 0.02, 0.025, 0.03, 0.035$, and 0.04 from bottom to top. For fixed angular momentum J, both the work and efficiency increase with T_1. On the other hand, the work and efficiency remain almost the same for different J when the high temperature T_1 is also fixed. The slight difference is that the work slightly decreases with J for $T_1 = 0.02, 0.025, 0.03$, and 0.035, while increases with J for $T_1 = 0.04$. However, the efficiency shows a slight increase with J for different high temperature T_1. One significant result from figure 9(b) is that for fixed J, increasing T_1 will greatly increase the efficiency for the engine.

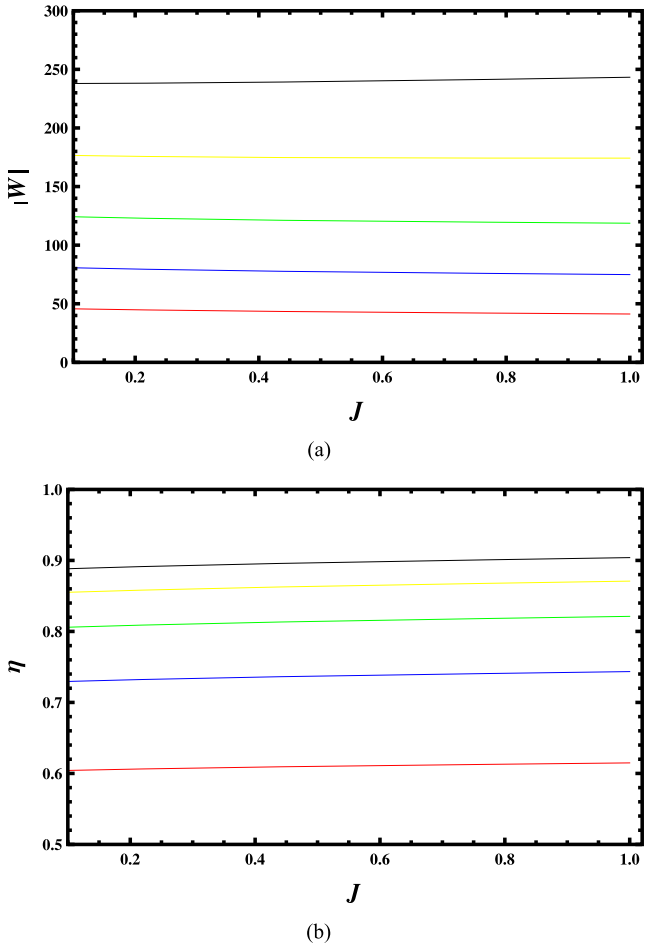

Figure 9. Work and efficiency as a function of the angular momentum J for the Rankine engine with the low temperature $T_2 = 0.01$, while with $T_1 = 0.2$, 0.25,0.3, 0.35, 0.4 from bottom to top. (a) Work $|W|$ versus J. (b) Efficiency η versus J.

5. Conclusions

In this paper, we have studied heat engines for the rotating Kerr-AdS black hole. First, we briefly reviewed the thermodynamics and phase structure of the rotating Kerr-AdS black hole. The thermal stability of Kerr-AdS black holes, along with their dependence on various parameters, have been thoroughly examined in this study. Afterward, we considered four thermodynamic processes: adiabatic, isothermal, isobaric, and isometric processes. The expressions of the heat absorbed or released from these processes were derived by using the first law of the black hole thermodynamics. Based on this, we studied the Carnot engine, Stirling engine, and Rankine engine. The work and efficiency for these black hole engines were obtained.

For the Carnot engine with fixed low temperature $T_2 = 0.01$, the work always has a maximum at a certain temperature. And the maximum work decreases with the angular momentum J. If both high and low temperatures are fixed, then both the heat and work decrease with the angular momentum. However, the efficiency for the Carnot engine is always $\eta = 1 - T_2/T_1$. For the Stirling engine, we found that the work decreases with the angular momentum. While for the same angular momentum, the work decreases with the high temperature. Moreover, we numerically studied the Rankine engine in detail. For fixed low temperature T_2, we found that both the work and efficiency of the heat engine increase with the high temperature T_1. Furthermore, for fixed low and high temperatures, the work and efficiency are almost identical, respectively. The work slightly decreases with J for low T_1, while increases for high T_1. On the other hand, the efficiency slightly increases with J. Nevertheless, we observed that the angular momentum has a significant influence on the black hole thermodynamics and heat engines.

Acknowledgments

This work was supported by the Natural Science Foundation of Hunan Province, China (Grant No. 2022JJ40033), and the National Natural Science Foundation of China (Grant No. 12 305 061).

References

[1] Caldarelli M M, Cognola G and Klemm D 2000 Thermodynamics of Kerr-Newman-AdS black holes and conformal field theories *Class. Quant. Grav.* **17** 399
[2] Cvetic M, Gibbons G, Kubiznak D and Pope C 2011 Black hole enthalpy and an entropy inequality for the thermodynamic volume *Phys. Rev.* D **84** 024037
[3] Lu H, Pang Y, Pope C N and Vazquez-Poritz J F 2012 Ads and lifshitz black holes in conformal and Einstein-Weyl gravities *Phys. Rev.* D **86** 044011
[4] Kastor D, Ray S and Traschen J 2009 Enthalpy and the mechanics of ads black holes *Class. Quant. Grav.* **26** 195011
[5] Dolan B P 2011 The cosmological constant and the black hole equation of state *Class. Quant. Grav.* **28** 125020
[6] Dolan B P 2011 Pressure and volume in the first law of black hole thermodynamics *Class. Quant. Grav.* **28** 235017
[7] Dolan B P 2011 Compressibility of rotating black holes *Phys. Rev.* D **84** 127503
[8] Kubiznak D and Mann R B 2012 P-V criticality of charged AdS black holes *J. High Energy Phys.* JHEP07(2012)033
[9] Kubiznak D, Mann R B and Teo M 2017 Black hole chemistry: thermodynamics with Lambda *Class. Quant. Grav.* **34** 063001
[10] Wei S-W and Liu Y-X 2015 Insight into the microscopic structure of an AdS black hole from thermodynamic phase transition *Phys. Rev. Lett.* **115** 111302
Wei S-W and Liu Y-X 2016 Erratum: Insight into the microscopic structure of an AdS black hole from a thermodynamical phase transition [Phys. Rev. Lett. 115, 111302 (2015)] *Phys. Rev. Lett.* **116** 169903
[11] Johnson C V 2014 Holographic heat engines *Class. Quant. Grav.* **31** 205002
[12] Johnson C V 2016 An exact efficiency formula for holographic heat engines *Entropy* **18** 120
[13] Belhaj A, Chabab M, EL Moumni H, Masmar K, Sedra M B and Segui A 2015 On heat properties of AdS black holes in higher dimensions *J. High Energy Phys.* JHEP05(2015)149
[14] Sadeghi J and Jafarzade K 2017 Heat engine of black holes *Int. J. Theor. Phys.* **56** 3387

[15] Caceres E, Nguyen P H and Pedraza J F 2015 Holographic entanglement entropy and the extended phase structure of STU black holes *J. High Energy Phys.* JHEP09(2015)184
[16] Setare M R and Adami H 2015 Polytropic black hole as a heat engine *Gen. Rel. Grav.* **47** 11
[17] Johnson C V 2016 Gauss-Bonnet black holes and holographic heat engines beyond large N *Class. Quant. Grav.* **33** 215009
[18] Johnson C V 2016 Born-Infeld AdS black holes as heat engines *Class. Quant. Grav.* **33** 135001
[19] Sadeghi J and Jafarzade K 2017 The modified Horava-Lifshitz black hole from holographic engine *Int. J. Mod. Phys.* D **26** 1750138
[20] Bhamidipati C and Yerra P K 2017 Heat engines for dilatonic born-infeld black holes *Eur. Phys. J.* C **77** 534
[21] Zhang M and Liu W-B 2016 $f(R)$ black holes as heat engines *Int. J. Theor. Phys.* **55** 5136
[22] Chakraborty A and Johnson C V 2019 Benchmarking black hole heat engines *Int. J. Mod. Phys.*D **28** 1950012
[23] Mo J-X, Liang F and Li G-Q 2017 Heat engine in the three-dimensional spacetime *J. High Energy Phys.* JHEP03(2017)010
[24] Hennigar R A, McCarthy F, Ballon A and Mann R B 2017 Holographic heat engines: general considerations and rotating black holes *Class. Quant. Grav.* **34** 175005
[25] Liu H and Meng X-H 2017 Effects of dark energy on the efficiency of charged AdS black holes as heat engine *Eur. Phys. J.*C **77** 556
[26] Johnson C V 2018 Taub-Bolt heat engines *Class. Quant. Grav.* **35** 045001
[27] Xu H, Sun Y and Zhao L 2017 Black hole thermodynamics and heat engines in conformal gravity *Int. J. Mod. Phys.* D **26** 1750151
[28] Bhamidipati C and Yerra P K 2017 A note on Gauss-Bonnet black holes at criticality *Phys. Lett.* B **772** 800
[29] Mo J-X and Li G-Q 2018 A note on Gauss-Bonnet black holes at criticality *J. High Energy Phys.* JHEP05(2018)122
[30] Hendi S H, Panah B E, Panahiyan S, Liu H and Meng X-H 2018 Black holes in massive gravity as heat engines *Phys. Lett.* B **781** 40
[31] Chakraborty A and Johnson C V 2019 Benchmarking black hole heat engines, II *Int. J. Mod. Phys.*D **28** 1950006
[32] Zhang J, Li Y and Yu H 2018 Accelerating AdS black holes as the holographic heat engines in a benchmarking scheme *Eur. Phys. J.* C **78** 645
[33] Graca J P M, Lobo I P, Bezerra V B and Moradpour H 2018 Effects of a string cloud on the criticality and efficiency of AdS black holes as heat engines *Eur. Phys. J.* C **78** 823
[34] Zhang J, Li Y and Yu H 2019 Thermodynamics of charged accelerating AdS black holes and holographic heat engines *J. High Energy Phys.* JHEP02(2019)144
[35] Li S-L and Wei H 2019 Holographic entanglement entropy and van der waals transitions in Einstein-Maxwell-Dilaton theory *Phys. Rev.* D **99** 064002
[36] Wei S-W and Liu Y-X 2019 Implementing black hole as efficient power plant *Commun. Theor. Phys.* **71** 711
[37] Wei S-W and Liu Y-X 2019 Charged AdS black hole heat engines *Nucl. Phys.* B **946** 114700
[38] Gunasekaran S, Kubiznak D and Mann R B 2012 Extended phase space thermodynamics for charged and rotating black holes and Born-Infeld vacuum polarization *J. High Energy Phys.* JHEP11(2012)110
[39] Altamirano N, Kubiznak D, Mann R B and Sherkatghanad Z 2014 Thermodynamics of rotating black holes and black rings: phase transitions and thermodynamic volume *Galaxies* **2** 89
[40] Roy T, Sardar A and Debnath U 2023 Thermodynamic overview and heat engine efficiency of Kerr–Sen–AdS black hole *Int. J. Geom. Meth. Mod. Phys.* **20** 2350136
[41] Ökcü Ö and Aydıner E 2018 Joule–Thomson expansion of Kerr–AdS black holes *Eur. Phys. J.* C **78** 123
[42] Gao Z, Kong X and Zhao L 2022 Thermodynamics of kerr-ads black holes in the restricted phase space *Eur. Phys. J.* C **82** 112
[43] Wei S-W, Cheng P and Liu Y-X 2016 Analytical and exact critical phenomena of d-dimensional singly spinning Kerr-AdS black holes *Phys. Rev.* D **93** 084015